

1 Upper Ocean Response on the Passage of Tropical Cyclones in 2 the Azores Region

3 Miguel M. Lima¹, Célia M. Gouveia^{1,2}, Ricardo M. Trigo^{1,3}

4 *Correspondence to:* Miguel M. Lima

5 ¹Instituto Dom Luiz (IDL), Faculdade de Ciências, Universidade de Lisboa, 1749-016, Lisboa, Portugal

6 ²Instituto Português do Mar e da Atmosfera (IPMA), I.P., 1749-077, Rua C do Aeroporto, Lisboa, Portugal

7 ³Departamento de Meteorologia, Universidade Federal do Rio de Janeiro, Rio de Janeiro 21941-919, Brasil

8 **Abstract.** Tropical Cyclones (TCs) are extreme climate events that are known to strongly interact with the ocean
9 through two mechanisms: dynamically through the associated intense wind stress, and thermodynamically through
10 moist enthalpy exchanges at the ocean surface. These interactions contribute to relevant oceanic responses during and
11 after the passage of a TC, namely the induction of a cold wake and the production of chlorophyll (Chl-a) blooms. This
12 study aimed to understand these interactions in the Azores region, an area with relatively low cyclonic activity for the
13 North Atlantic basin, since the area experiences much less intense events than the rest of the basin. Results for the
14 1998-2020 period showed that the averaged induced anomalies were on the order of $+0.050 \text{ mg m}^{-3}$ for the Chl-a and
15 -1.615 K for SST. Furthermore, looking at the role played by several TCs characteristics we found that the intensity
16 of the TCs was the most important condition for the development of upper ocean responses. Additionally, it was found
17 that bigger TCs induced greater anomalies in both variables, while faster ones created greater Chl-a responses, and
18 TCs that occurred later in the season had greater anomalies. Two case studies (Ophelia, in 2017, and Nadine, in 2012)
19 were conducted to better understand each upper ocean response. Ophelia showed to affect the SST at an earlier stage
20 while the biggest Chl-a induced anomalies were registered at a later stage, allowing the conclusion that thermodynamic
21 exchanges conditioned the SST more while dynamical mixing might have played a more important role in the later
22 stage. Nadine showed the importance of the TC track geometry, revealing that the TC track observed in each event
23 can impact a specific region for longer, and therefore induce greater anomalies.

24 **Introduction**

25 Tropical Cyclones (TCs) are potentially intense atmospheric disturbances which are characterised by a low-pressure
26 centre (eye) where strong winds curl around. Among other important properties, TCs are thermodynamic dependent
27 phenomena, meaning that intense temperature gradients need to occur in the lower atmosphere to maintain and
28 intensify the storm. Thus, TCs are fed from warm sea water which provide a strong moist enthalpy flux from the
29 oceanic surface to maintain a steep temperature gradient within the lower and middle troposphere and produce massive
30 water vapour convection (Emanuel, 2003; Holton and Hakim, 2012; Pearce, 1987).

31 The strong wind stress present near the surface and the associated intense curl are also shown to induce vertical mixing
32 and Ekman upwelling in the upper layer of the ocean. In his seminal study, Price (1981) shows, through both observed
33 and numerical modelling data, the evolution of sea surface temperature (SST) on the passage of a hurricane, with the
34 emergence of a cold wake of SST after a TC due to entrainment of water from shallow layers. This effect has since
35 been well studied and documented with many case studies observed, for example, the case of Hurricane Felix, in the
36 vicinity of Bermuda in 1995, that showed decreases in the order of 3.5-4 °C (Dickey *et al.*, 1998), or the cases of
37 cyclones Nargis (2008) and Laila (2010), in the Bay of Bengal, that caused SSTs to drop by around 1.76 °C (Maneesha
38 *et al.*, 2012). Additionally, several model-based works focused on either the effects caused by the TCs, or the
39 interaction of the TC with its own cold wake (e.g., Chen *et al.*, 2017; Zhang *et al.*, 2019).

40 There are also biological responses to the passage of a TC. Due to the upwelling of colder water, transport of nutrient-
41 rich water from the sub-superficial layer may also occur (Kawai and Wada, 2011). In this case, phytoplankton can
42 quickly increase in the surface layer following the rise in nutrients. This increase can be remotely sensed through
43 satellite observations that capture the chlorophyll-a concentration (Chl-a) increasing after the passage of a TC, since
44 Chl-a is generally accepted as a proxy for biological activity (Kawai and Wada, 2011; Liu *et al.*, 2009; Subrahmanyam
45 *et al.*, 2002; Walker *et al.*, 2005).

46 The oceanic response, either physical or biological, to the passage of a TC depends on various aspects, most
47 remarkably the TC's intensity and its translation speed but also the oceanic subsurface conditions (Zheng *et al.*, 2008).
48 The magnitude and significance of these aspects on the modulation of the oceanic response varies regionally, although
49 it is generally regarded that the most impactful phenomena to be those of an intense and slow TC (Chacko, 2019;
50 Price, 1981; Price *et al.*, 1994). Recent studies (e.g., Chacko, 2019; Pan *et al.*, 2018; Shropshire *et al.*, 2016) have
51 shown that regional differences do matter when studying the biological response. In the case of the Bay of Bengal, it
52 was shown that the intensity of a TC is less important, and the most meaningful aspects are the TC's translation speed
53 and, to a lesser degree, a pre-existing shallow mixed layer (Chacko 2019). The results from this study are important
54 to stress that relatively weaker TCs can also induce a strong biological response after their passage.

55 Until now, the Azores region has not been studied regarding its thermodynamic and biological impacts. This section
56 of the North Atlantic basin presents much fewer and weaker cyclones than the tropical band of the basin, with this
57 region being mainly a zone where TCs undergo either cyclosis or post-tropical transition into extra-tropical cyclones
58 or mid-latitude storms (Baatsen *et al.*, 2015; Haarsma *et al.*, 2013). The north-eastern Atlantic (NEA) basin, where the
59 Azores archipelago is located, presents significantly less TCs than the western counterpart, closer to the USA coast
60 (Baatsen *et al.*, 2015; Lima *et al.*, 2021; Haarsma *et al.*, 2013). However, there is growing evidence of a significant
61 increase in the frequency of strong TCs in both western (Kossin *et al.*, 2020) and eastern (Lima *et al.*, 2021) halves of
62 the north Atlantic Ocean. The climatology of the area points to a south-north gradient in both SST and Chl-a, with a
63 decrease in the former and an increase in the latter (Amorim *et al.*, 2017; Caldeira and Reis, 2017). In general, the
64 southern part of the Azores region offers SSTs high enough to maintain TCs, although the necessary atmospheric
65 conditions (e.g., high lapse rates and low wind shear) need to occur for their passage northeast through the Azores

66 (Lima et al., 2021). However, this area is undergoing a transition due to anthropogenic climate change and an increase
67 both in number and intensity of TCs is expected (Baatsen et al., 2015; Haarsma et al., 2013). Therefore, the NEA basin
68 is a challenging study region to assess the impact that lower intensity TCs have on the oceanic surface.

69 The main aim of this study is to analyse in detail the upper ocean response observed after the passage of a TC in the
70 Azores region, which is characterised by its lower-than-normal cyclonic activity in relation to the rest of the north
71 Atlantic basin. In particular, we aim to evaluate the impacts on SST and Chl-a concentration produced by important
72 TC characteristics (averaged maximum wind speed, average translation speed, overall impacted area, time of
73 occurrence, and geometry of the track). Two practical case studies, relative to Nadine (2012) and Ophelia (2017) are
74 then thoroughly analysed to reflect the drawn conclusions for this area.

75 **Data**

76 The main data used to evaluate the oceanic response in this study is divided into three main parts: Remotely sensed
77 interpolated data used to characterise the Chl-a and SST, respectively, and TC track data, which provides the necessary
78 additional information on the location and dynamic variables of each TC, that allow to explore the oceanic response
79 in the aforementioned data. Additionally, non-interpolated datasets are used for the case studies to validate the
80 interpolated ones; and wind-stress data is used for the Hurricane Ophelia study case.

81 Biological oceanic response was evaluated using a multi-sensor daily Chl-a product available through the Copernicus
82 Marine Environment Monitoring Service (CMEMS) in a 4 km x 4 km resolution from the end of 1997 to the present
83 (CMEMS, 2021b). This product, delivered by the ACRI-ST company, is based on the Copernicus-GlobColour project
84 and obtained by merging different sensors: SeaWiFS, MODIS, MERIS, VIIRS-SNPP&JPSS1, OLCI-S3A&S3B. The
85 final Chl-a product is a mix of several algorithms that consider different water conditions, such as oligotrophic,
86 mesotrophic, coastal, clear, and complex waters (Garnesson et al., 2019). To produce a “cloud free” product, the
87 resulting data was subjected to daily interpolation to fill any gaps (Krasnopolsky et al., 2016; Saulquin et al., 2019).
88 The lack of gaps in this dataset is particularly relevant in the context of this study since the areas analysed will be
89 concentrated around the TCs; it is then expected that large amounts of the analysed areas would be under cloud
90 coverage and, therefore, some of the analysed data is not real but interpolated values. Nonetheless, CMEMS provides
91 approximate uncertainty levels for this data, which we used to assess the quality of our results. For further validation
92 purposes we used also a non-interpolated Chl-a product generated by the Ocean Colour component of the European
93 Space Agency’s Climate Change Initiative project (OC-CCI) (Sathyendranath et al., 2019). This dataset results from
94 a merge of several sensors: SeaWiFS LAC and GAC, MODIS Aqua, MERIS, VIIRS, and OLCI. ESA’s OCC-CI
95 version 5.0 Chl-a product has 0.042° resolution and a daily temporal resolution (Sathyendranath et al., 2021).

96 To evaluate the physical oceanic response and to relate this to the biological one, a daily SST dataset from the CMEMS
97 was used, with a 0.05° resolution. This data is available from 1981 up to the near present (CMEMS, 2021a). Similarly,
98 to the previous CMEMS interpolated Chl-a product the SST field is also a blended gap-free analysis product, with the
99 present one resulting from re-processed (A)ATSR, SLSTR and AVHRR sensor data being applied to the Operational

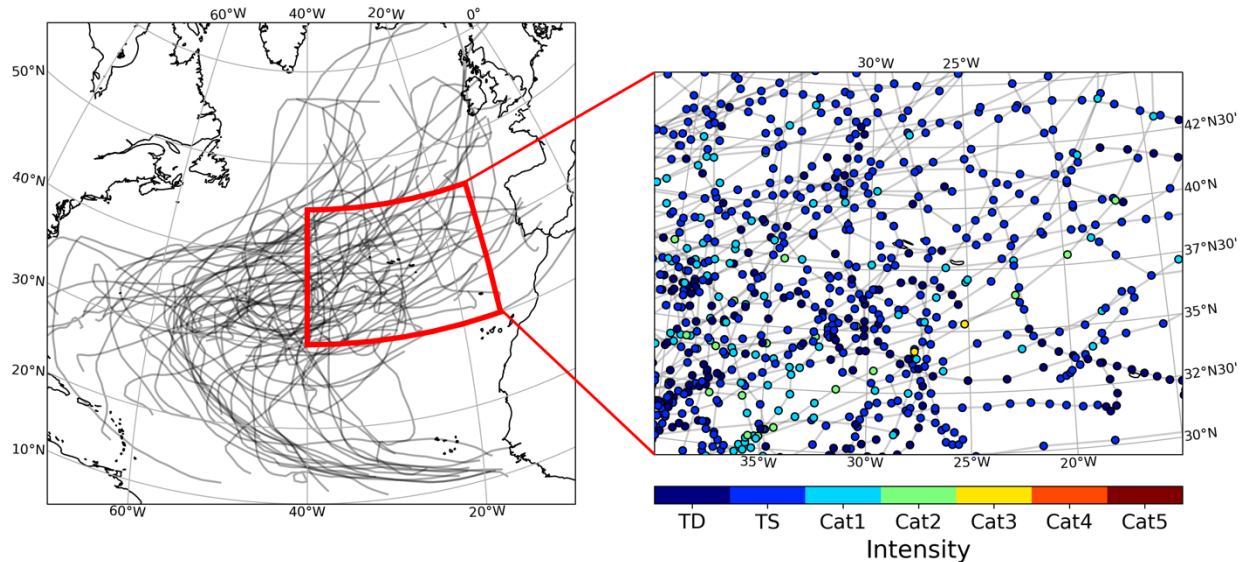
100 SST and Sea Ice Analysis (OSTIA) system (Donlon et al., 2012). This reprocessed analysis product provides an
101 estimate of the SST at 20 cm depth. The inputs to the system are SSTs at 10:30 am and 10.30 pm local time which
102 means that the analyses roughly correspond to the daily average SST (Good et al., 2020; Lavergne et al., 2019;
103 Merchant et al., 2013). As stated before, approximated error values for SST are also provided by CMEMS.
104 Additionally, AVHRR Pathfinder version 5.3 collated data was used as non-interpolated data for validation. This
105 dataset, similarly to the CMEMS one, is a collection of twice-daily (averaged to daily), 4km spatial resolution, merged
106 SST product, provided by NOAA's National Centers for Environmental Information (Saha et al., 2018). The merge
107 of this data, however, is only used to spatially collate the data, as it is a single instrument measurement (AVHRR)
108 onboard NOAA-7 through NOAA-19 Polar Operational Environmental Satellites (POES).

109 Wind stress data to assist in the analysis of the Hurricane Ophelia study case was provided by NOAA's CoastWatch
110 dataset available at https://coastwatch.pfeg.noaa.gov/erddap/griddap/erdQMstress1day_LonPM180.html. This dataset
111 is derived from wind measurements obtained from the Advanced Scatterometer (ASCAT) instrument on board
112 EUMETSAT's MetOp satellites (A and B) at a daily 0.25° resolution, from 2013 to the present. ASCAT presents a
113 near all-weather capacity (not affected by clouds), as it operates a frequency in C-band (5.255 GHz), therefore,
114 minimizing the number of missing values in predominately clouded areas such as the case of TC paths.

115 The TC track data is made available by the *International Best Track Archive for Climate Stewardship Project* version
116 4 (IBTrACS v4) free access dataset (Knapp et al., 2009). This dataset contains global information regarding TC
117 activity since the 1851 hurricane season up to 2020. It aggregates variables such as TC geographical location,
118 maximum wind speed, minimum sea level pressure, and storm radius estimation based on wind intensity, measured at
119 6-hour intervals (original dataset interpolates for increased resolution, at 3-hour rates, however this interpolation only
120 includes the geographical location). For the 1998-2020 period, the Azores region experienced the passage of 62
121 individual TCs accounting to 642 6-hour observations that are categorised in the following intensities according to the
122 Saffir-Simpson hurricane wind scale (Taylor et al., 2010):

- 123 ● 148 tropical depression observations.
- 124 ● 389 tropical storm observations.
- 125 ● 85 category 1 hurricane observations.
- 126 ● 18 category 2 hurricane observations.
- 127 ● 2 category 3 hurricane observations.

128 The full TC tracks can be better visualised in Fig. 1, with the left panel showing the full track for all these 62 TCs'
129 observed in the NA basin for the 1998-2020 period and the right panel showing a zoomed view relative to the
130 considered Azores region. Tropical depression observations (dark blue in Fig. 1, right panel) account for 23 % of the
131 total observations and will not be considered in this study, as they present the lower branch of intensities with winds
132 below the 34-kt (18 m/s) threshold. Therefore, a total of 494 TC 6-hour observations were considered for this study.



133
 134 **Figure 1 - Left panel: North Atlantic basin and the tracks for all TCs that went through or occurred inside the study region**
 135 **(shown by the red outline). Right panel: Zoom of the previous red outline, with each TC observation marked in different**
 136 **colours for intensity (TD: Tropical Depression; TS: Tropical Storm; Cat1 - Cat5: Hurricane category according to the**
 137 **hurricane Saffir-Simpson wind scale).**

138 Since the interpolated datasets used for most of this study do not share the same time frame and to better encapsulate
 139 full years of data, the timeframe of the present study will be from January 1st of 1998 to December 31st of 2020.
 140 Moreover, while we have extracted all the data described above covering the entire North Atlantic basin, we will focus
 141 on the area around the Azores archipelago, delimited by the 15°W and 40°W meridians and between the 30°N and the
 142 45° parallels (Fig. 1).

143 **Methodology**

144 The region of study was chosen due to its nature regarding TCs, since it is an area with fewer and less intense tropical
 145 storms (Hart and Evans, 2001; Lima et al., 2021; Ramsay, 2017). Generally, tropical cyclosis and post-tropical
 146 transition occur here (Baatsen et al., 2015; Haarsma et al., 2013). Because of these aspects, it corresponds to a much
 147 less studied area and is a good region to characterise oceanic biophysical effects after the passage of (generally) weaker
 148 TCs at higher-than-tropical latitudes and to compare the obtained results with previous literature.

149 To cope with large amounts of data, the bio-physical response was evaluated within a small area around individual
 150 locations obtained for each TCs' best-track location. For this, we used the approximated quadrant radius given by the
 151 IBTrACS v4 dataset. This dataset provides different types of radii depending on the considered isotach, for this study
 152 we used the 34-kt isotach as it corresponds to the lower-bound for the Tropical Storm status according to the Saffir-
 153 Simpson hurricane wind scale (Taylor et al., 2010). Since the considered area of analysis falls above the 34-kt isotach,
 154 tropical depressions were not considered (exact partition of intensities is given at the beginning of the *Results* section).
 155 There are some missing radii values in the middle of TC tracks and in order to correct a simple linear regression was

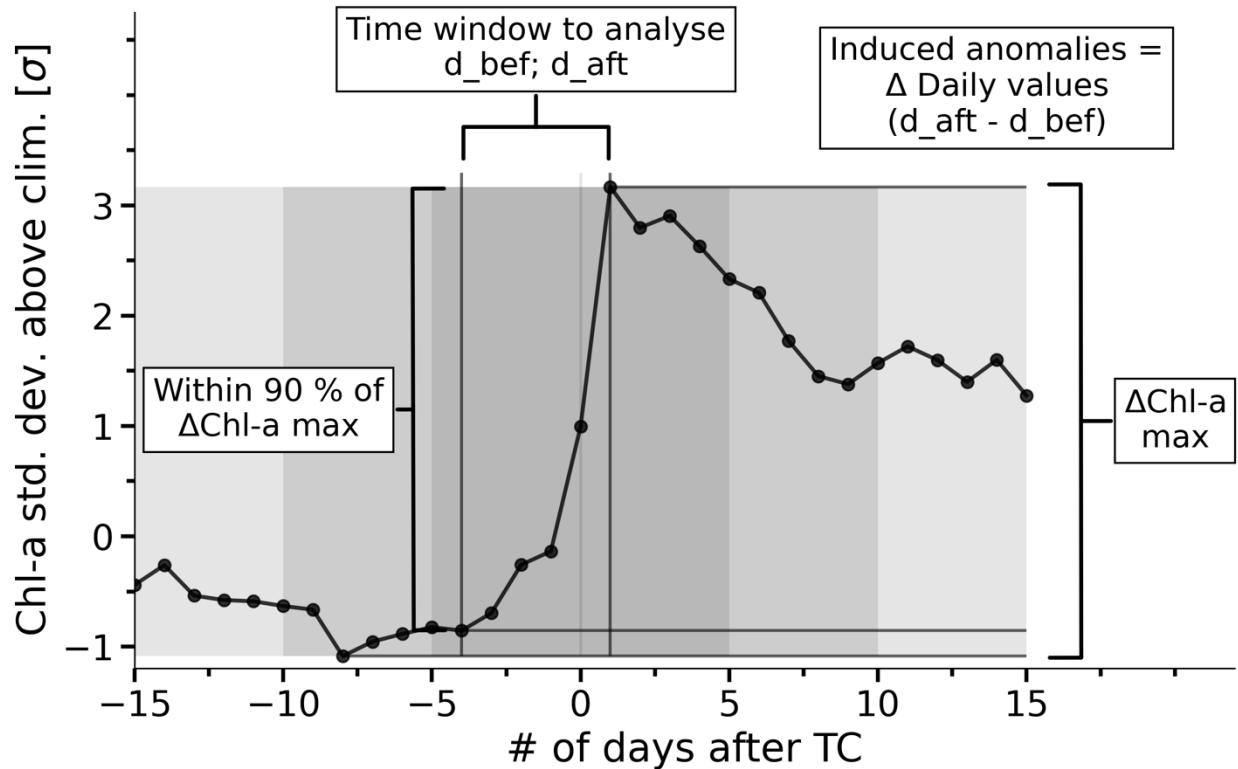
156 applied. To illustrate the application of this methodology we present the study cases in the *results and discussion*
157 section, for hurricanes Ophelia (2017) and Nadine (2012). From inside this area of analysis, we may retrieve the Chl-
158 a concentration and SST at their respective resolution. The analysis inside the considered area was performed using
159 histograms, in which each pixel inside the 34-kt isotach contributes to that TCs histogram.

160 To analyse the TCs' impact on their passage, inspiration was taken from Kawai and Wada (2011), who computed the
161 climatic monthly standard deviation of Chl-a on 0.25° grids over a 5-year study period. Here, we computed for each
162 storm the daily standard deviation of both Chl-a and SST over their respective grids relative to the climatology over
163 the same area (only the area impacted by the TC was considered) for the study's complete time frame; this analysis
164 was performed considering 30 days before and after each TC to allow then the analysis of an ideal window to compute
165 the induced anomalies. To compute this ideal window, we searched for the maximum difference between the number
166 of standard deviations over the climatological value before and after the storm.

167 To compromise between having the maximum difference and ensuring a time window as close as possible to the storm
168 (to minimize external factors to the TC), we performed a sensibility study on the length and location of the considered
169 time window. First, we analyse the overall maximum difference in the 61-day period (including the day of the storm)
170 and then search for a secondary maximum value that is within 10% of it considering a smaller sample of days,
171 decreasing in groups of 5 days each time this search is made (e.g., the first iteration would be 25 days before and 30
172 after, the second 30 before and 25 after, the third 25 before and after, etc.), until an optimum maximum difference
173 value is identified. With this window defined, the induced anomalies are simply the difference between the daily
174 values of Chl-a or SST after and before the TC.

175 As an example of this methodology, Fig. 2 shows the Chl-a standard deviation over the climatological value in the
176 case of Hurricane Nadine. In this case, only 15 days around the TC are shown for clarity. We can see that the maximum
177 difference is obtained between 8 days before and 1 day after the storm ($\Delta\text{Chl-a max}$). However, when we take into
178 account the compromise of considering windows located as close as possible to the occurrence of the TC over the
179 region, we see that the value found between 4 days before and 1 day after is within 10% of the absolute maximum.
180 This methodology is then applied to all 6-hour observations individually and for each TC, thus resulting in two groups
181 of induced anomalies (per TC and per 6-hour observations) where we can study these with respect to the TCs averaged
182 (per TC) or instantaneous (6-observations) characteristics.

183 To address the possibility that some pixels are overlaid on top of each other, which would contaminate the analysis,
184 as observed in the case of the slow erratic Hurricane Nadine (presented in the *results and discussion* section as a study
185 case), we did not take into consideration the days in which the TC is over the aforementioned overlaid region. In these
186 cases, the days considered are those when the TC has completely travelled over the area (i.e., that pixel is no longer
187 inside the radius of influence of the TC). However, when we consider independent 6-hour observations, this caveat
188 cannot be accounted for since we have no way of knowing if that area has been influenced or not by the TC before,
189 for how long, or even if a future observation will impact the area.



190

191 **Figure 2 - Schematic of the applied methodology for each TC. Black line shows the number of standard deviations from the**
 192 **climatological values for the area surrounding Hurricane Nadine. A detailed description of this methodology can be found**
 193 **in the text.**

194 As previously mentioned in the *Data* section, the interpolated data used for this study is expected to encounter some
 195 regions where clouds are to be expected due to the presence of the TCs. To account for this potential caveat, we looked
 196 at the uncertainties associated with the data before and after the TCs, as well as during the TC (e.g., day 0 in Fig. 2),
 197 to evaluate if there were clear increases in uncertainty for cloud covered situations.

198 Two case studies were looked at in greater detail: Hurricane Ophelia (2017) and Hurricane Nadine (2012). The former
 199 was performed to assess the different impacts along the lifecycle of the storm, and different histograms were produced
 200 for smaller portions of the TC. The latter was made to analyse the possible increasing impacts the storm geometry
 201 could cause. Additionally, these study cases were used as validation for the interpolated “cloud-free” data, where a
 202 comparison was made between the non-interpolated and the interpolated “cloud-free” data described in the *Data*
 203 section.

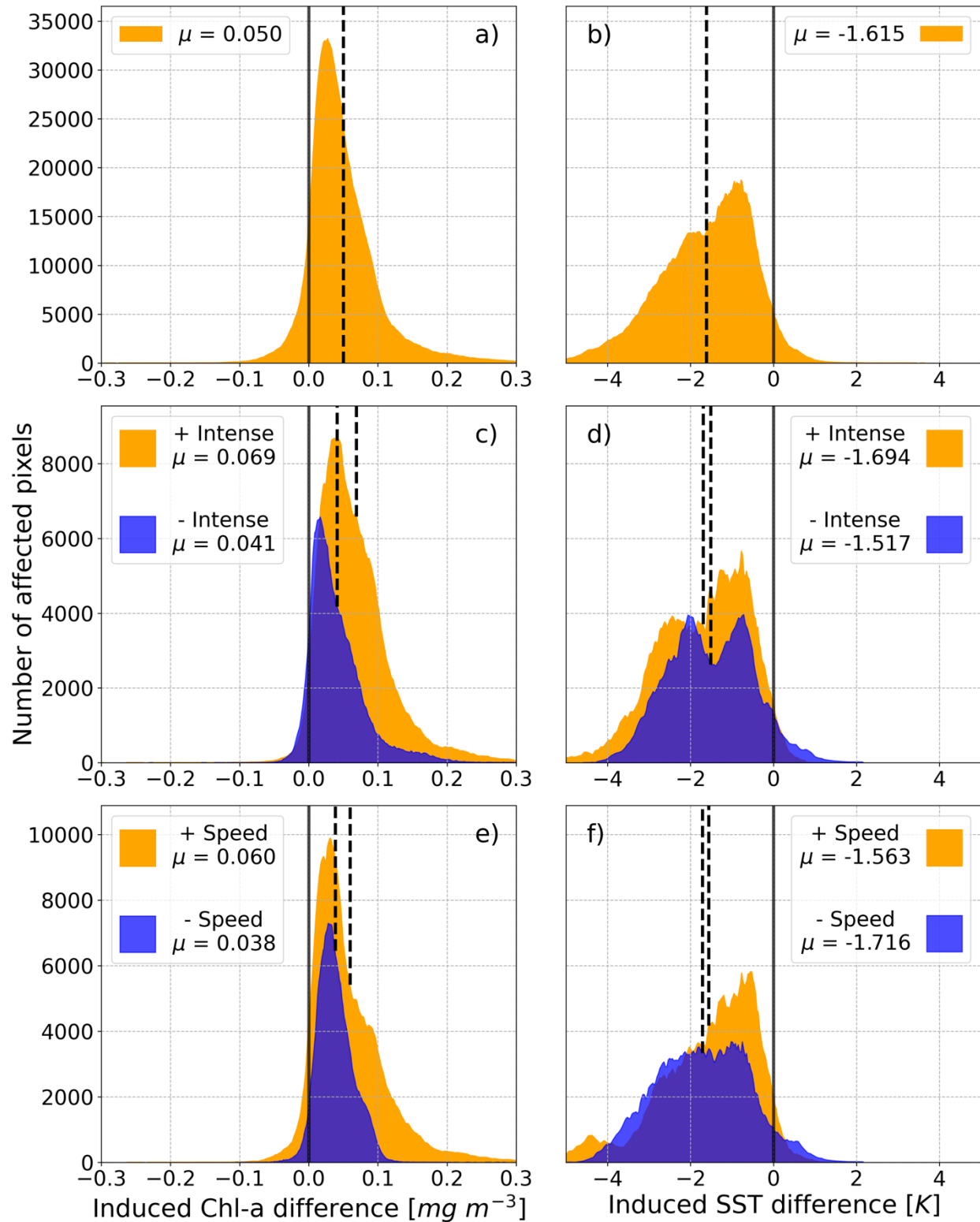
204 **Results and Discussion**

205 Applying the mentioned methodology leaves us with a large pool of induced anomalies, from which we can now
 206 evaluate the distribution of anomalies for both the Chl-a and SST as shown in Figs. 3a and 3b in the form of histograms
 207 of induced Chl-a and SST anomalies, respectively. Both variables present a large impact after the passage of TCs,

208 with the Chl-a presenting a mean response of positive 0.050 mg m^{-3} and the SST showing a mean response of negative
209 1.615 K . Figs. 3c-f show the corresponding distributions as a function of the cyclone's intensities (Figs. 3c and 3d)
210 and translation speeds (Figs. 3e and 3f). To make these distinctions, we chose only the high values (either regarding
211 intensity or translation speed) to be those above the third quartile and the lower values to be those below the second
212 quartile.

213 Firstly, regarding intensity (Figs. 3c and 3d), we have the induced response of the most powerful intensities in orange
214 and the weaker ones in blue. Regarding the impact as a function of intensity it is possible to observe that more powerful
215 TCs tend to induce a stronger biological response than weaker ones, which have a mean response closer to zero. It is
216 also important to note that the more powerful TCs have a response that is much more skewed towards extreme positive
217 values of Chl-a. Fig. 3d also shows a great impact regarding different intensities in SST, in which even weaker TCs
218 show a substantial mean response of -1.517 K and nearly all the analysed pixels showing negative induced anomalies.
219 Important to note the nearly bimodal nature of this distribution, which can be attributed to both the earlier phase of
220 TCs (more energy being drawn from the ocean) resulting in more negative SST values, and the less negative
221 corresponding to the later part of TCs since baroclinic instabilities are more prevalent than the action of moist enthalpy
222 flux from the ocean at this phase (Baatsen et al., 2015; Emanuel, 2003). Powerful TCs induced a more varied
223 distribution of anomalies, with a mean response of -1.694 K .

224 Regarding the different translation speeds, Fig. 3e shows that, for biological responses, faster TCs show a greater
225 mean value of $+0.060 \text{ mg m}^{-3}$. This difference is not as expressive as the one in Fig. 3c. On the other hand, the SST
226 response (Fig. 3f) seems to be weakly impacted by the TC's translation speed, with slower TCs have a slightly stronger
227 impact than faster ones, while the mean response values do not differ as much as the ones in Fig. 3d. Additionally,
228 even if faster TCs do not affect the SST response as much as slower ones, the mean value is still close to what is seen
229 in the general case in Fig. 3b, and most of the impact is towards negative SSTs.

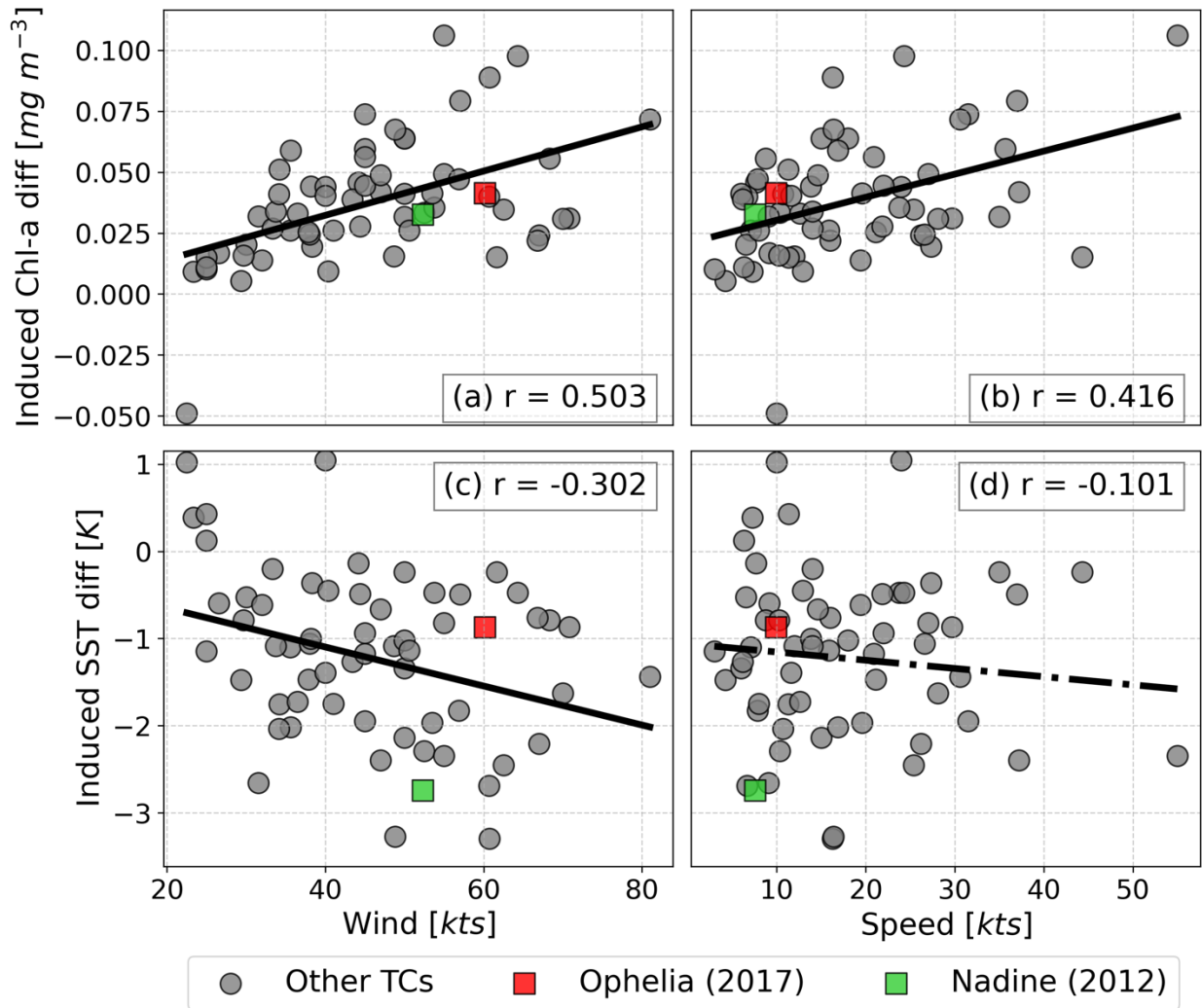


230

231 **Figure 3 - Histograms for the: a) Total Chl-a and b) SST induced anomalies; c) Chl-a and d) SST induced anomalies after**
 232 **weak (blue) and powerful TCs (orange); e) Chl-a and f) SST induced anomalies after slow TCs (blue) and fast TCs (orange).**

233 Each subplot histogram presents the respective population mean value (μ) in a dashed black line, and the zero value on a
 234 grey line.

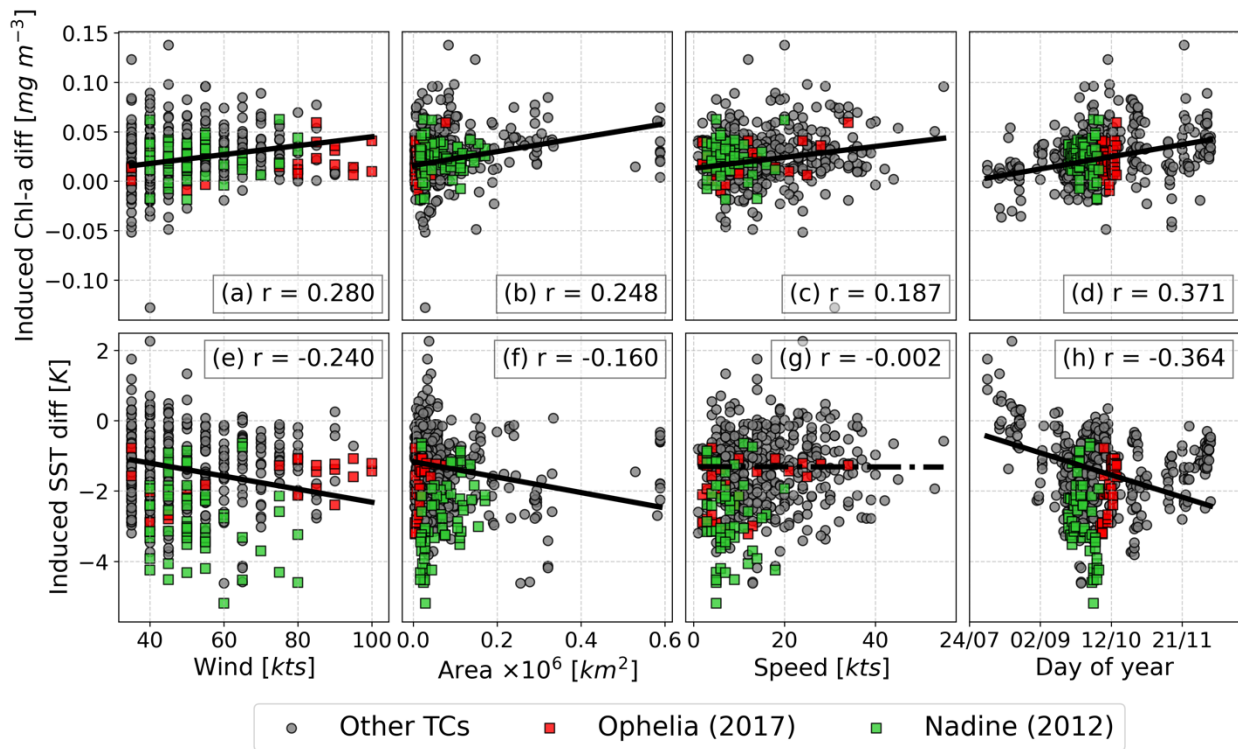
235 To quantify these relations, Fig. 4 shows the storm-averaged induced anomalies compared to the averaged maximum
 236 wind and average translation speed. The linear regression is also shown for each of the comparisons, with nearly all
 237 results significant at the 95 % statistical level. According to these plots, only the translation speed in relation to the
 238 SST induced anomalies (Figs. 4d) did not show a significant relation at the 95 % statistical confidence level (marked
 239 by the dashed regression line). Regarding the mean wind (Figs. 4a and 4c), and therefore the TC's average intensity
 240 within the Azores region, the linear regression showed significantly high values, upwards of 0.5 for Chl-a and -0.3 for
 241 SST induced anomalies. In the case of Chl-a, like observed in Fig. 3, the relation is positive while with SST this
 242 relation is negative. Considering the translation speed, the relation is equally positive and significant for biological
 243 responses ($r = 0.416$).



244
 245 **Figure 4 - Linear regression of Chl-a (top panel) and SST (bottom panel) induced anomalies for each TC, respectively, when**
 246 **compared with average winds in knots (left column); and average TC translation speed in knots (right column). In each**

247 plot the Pearson R is presented, and the regression's significance is marked by the type of line used in the regression, with
 248 a dashed line representing non-significant at a 95 % confidence level, and a solid line representing a regression significant
 249 at the 95 % confidence level.

250 Further analysis of other TC characteristics requires a different approach, Fig. 5 shows similar relations to Fig. 4, but
 251 considering 6-hour observations instead of total TC mean values. This is made to account for the possible error that
 252 averaging a whole TC may create since the cyclone's characteristics may change substantially along its lifetime. This
 253 analysis, however, does not consider the possibility of superposition in pixels from observation to observation – i.e.,
 254 from a TC that either moves slowly or whose track is more erratic, ending up covering the same area for several
 255 hours/days. This caveat was not present in Fig. 4 since we considered the TC lifetime as a whole and could then
 256 disregard the days of superposition. Using 6-hour observations, we can study several types of characteristics that
 257 change between observations, such as the impact area or the time of season when it occurred, adding to the already
 258 seen maximum wind speed and translation speed.



259
 260 **Figure 5 – Same as in Fig. 5 but considering individual 6-hour observations. Two columns are added: (b) and (f) with respect**
 261 **to the area affected by that observation; and (d) and (h) with respect to the time of the season when that observation**
 262 **occurred.**

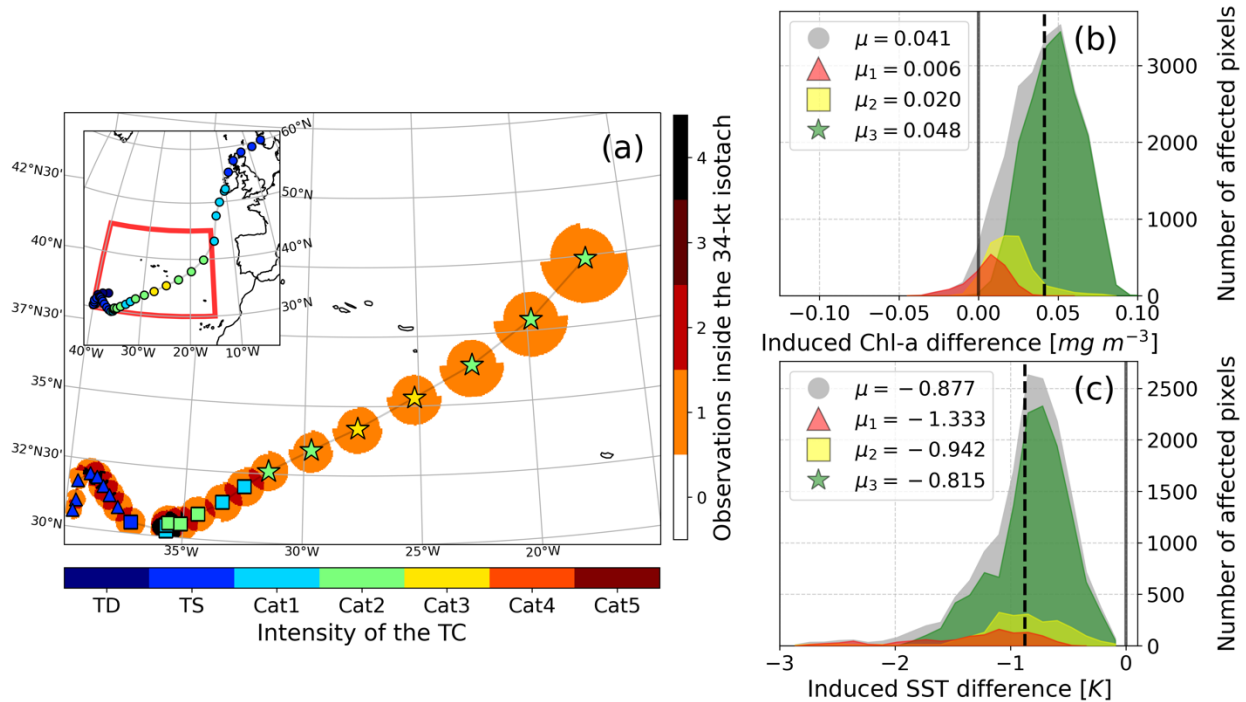
263 Considering then the maximum wind speed per observation (Fig. 5a and 5e), both variables are significantly related
 264 to this characteristic, which is expected considering the analysis made in Figs. 3 and 4. As previously noted in the
 265 form of histograms in Fig. 3, most observations show a positive impact regarding Chl-a and, especially for SST as
 266 most fall below zero, a negative change after a TC. The affected area (Figs. 5b and 5f) also presents a significant

267 relation, although less intense than that observed with the maximum winds. However, it should be noted that this
268 variable is linked to the mean winds, since more intense cyclones tend to be larger than less powerful ones, but also
269 to the storm phase, since storms nearing their post-tropical transition tend to grow larger (Knaff et al., 2014).
270 Translation speed is the less correlated variable from those studied (Fig. 5c and 5g), with only the biological response
271 seeing a positive relation to this characteristic, agreeing with the previous results from Figs. 3 and 4. The time period
272 in the season in which the TC occurs seems to also be important for the magnitude of the average induced anomaly
273 seen in both variables (Figs. 5d and 5h) with late occurrences in the season showing greater responses respective to
274 the signal of induced anomalies seen in Figs. 3a and 3b. Lastly, a geographical correlation was concluded not to be
275 relevant for this study (not shown), as both variables were correlated with both latitude and longitude, and only
276 negligible and non-significant relations were found.

277 The results presented so far in this study result from interpolated “cloud-free” data and should be quality assured to
278 guarantee the integrity of the conclusions made previously. As mentioned in the *Data* section, CMEMS provides
279 measures of uncertainty for the used Chl-a and SST datasets, thus, we have explored these values at different periods
280 as a first step in validating the quality of the data. Figure S1 shows the associated uncertainty with respect to the
281 absolute observed values both for Chl-a (top panels) and SST (bottom panels) for three different periods surrounding
282 a TC event (before, during, and after), and a randomly drawn sample of the same size as the data analysed in the other
283 subplots. It becomes immediately clear from these plots the considerably different magnitude of uncertainty for this
284 data, with Chl-a (Figs. S1a-d) ranging from 25 % to 45 % considering all moments, while SST (Fig. S1e-h) does not
285 commonly surpass 0.4 % with a mean error around the 0.25 %. The randomly drawn sample of data gives a rough
286 idea of the average uncertainty we can find in this dataset, with Chl-a (Fig. S1a) presenting values around 35 % and
287 SST (Fig. S1e) around 0.25 %. Additionally, we should consider three distinct moments of analysis, namely before
288 and after the TC passage, which corresponds to the data used to compute the induced anomalies, and during the TCs,
289 which should be the moment with most cloud-cover over the studied regions. Looking first at Chl-a (Figs. S1b-d) we
290 see the progression from near normal uncertainty before the TC (Fig. S1b) to an increase during TCs (Figs. S1c),
291 maybe due to the higher cloud-covered area in this situation, after the storm (Fig. S1d) however, the uncertainty
292 substantially decreases reaching values below the randomly drawn sample (around 30 % compared to 35 %). For the
293 SST (Figs. S1f-h), the associated uncertainty does not fluctuate substantially, constantly being below the 0.3 % mark.
294 Additionally, it is noticeable in both variables the variation that has been identified before, with Chl-a increasing and
295 the SST decreasing.

296 Visible in Figs. 4 and 5 are two case studies are marked: Hurricane Ophelia in 2017 (red squares) and Hurricane
297 Nadine in 2012 (green squares). These case studies were chosen based on the presented characteristics, coupled with
298 the amount of sampling data within the region. Hurricane Ophelia (2017) was chosen due to its large intensity in the
299 region (Red squares, Fig. 4 and 5), reaching a category 3 intensity in the Saffir-Simpson hurricane wind scale,
300 something abnormal for the region (Lima *et al.*, 2021). The complete TC track can be seen in Fig. 6a inset. Besides
301 the large intensity, Ophelia’s genesis took place inside our study region which enabled us to study different phases of
302 the storm and its impacts on the ocean surface in the region. Even though hurricane Ophelia was so intense, this storm

303 impacted a very small area (Figs. 5b and 5f) particularly when compared with the other case study, Hurricane Nadine
 304 (2012). Hurricane Nadine (Fig. 7a) was chosen due to its large sampling, relatively high intensity (maximum category
 305 1) and great impact area (second highest in this study, considering cumulative area of impact). The large impacted
 306 area was amplified by the geometry of the storm's track (i.e., many overlaid observations). Only the final stage of
 307 Hurricane Nadine was caught within the study region, producing an ideal case study to analyse the impact of a less
 308 intense storm that heavily impacted a particular region due to its geometry.

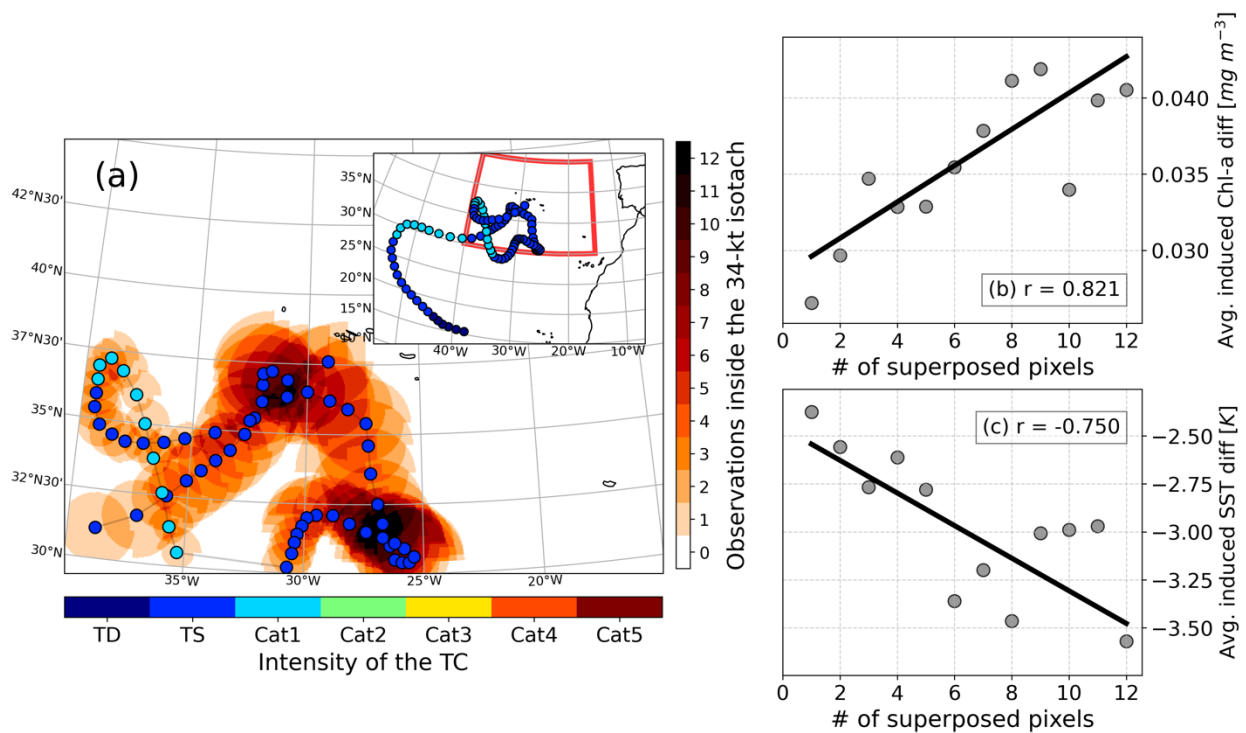


309
 310 **Figure 6 - Case study for Hurricane Ophelia, in 2017, with its track on the left panel (scatter marker colour scheme**
 311 **represents intensity as in Fig. 1), as well as the affected area around the cyclone (marked as the 34-kt isotach) with shading**
 312 **according to the number of pixels overlapping. Inside, there is an inset with the full track and the region of study marked**
 313 **with a red box. Ophelia track is divided in three phases: Histograms show induced Chl-a (b) and SST anomalies (c), by**
 314 **phase of the storm (colours) and in total (grey). The phase of the storm is marked in (a) as triangles (genesis), squares**
 315 **(maturing), and stars (mature) and correspond to the aforementioned colours in (b) and (c).**

316 For the case study of Hurricane Ophelia (2017), three different phases of the storm were studied, corresponding
 317 approximately to: cyclogenesis (Fig. 6a, triangles), maturing (Fig. 6a, squares), and mature hurricane (Fig. 6a, stars).
 318 There are 23 total observations; the first two phases encompass 8 observations and the last one 7. Each of these phases
 319 has its own histogram in Figs. 6b and 6c (shown in colours), for the induced Chl-a and SST anomalies, respectively.
 320 The histograms are inserted in a larger one (in grey), representing the total induced anomalies caused by Ophelia and
 321 therefore, the sum of all three phases will result in the bigger histogram. Regarding the Chl-a induced anomalies (Fig.
 322 6b), Ophelia seemed to have a higher impact towards the end of its track in the region of study, when the storm had
 323 the highest intensity and the mean values of the induced anomalies increased along the track. Even at the storm's
 324 genesis, the induced anomalies were mostly positive with a mean value of +0.006 mg m⁻³ reaching +0.048 mg m⁻³ in

325 the most intense phase. In contrast, the SST induced anomalies (Fig. 6c) present the highest mean response (-1.333
 326 K) at the initial phase. The SST induced anomaly is then seen decreasing as the storm goes on, with the last phase
 327 weighing the most in the general distribution (as was seen for the Chl-a). The highest SST impact of the storm during
 328 the initial phases may reflect that this is the phase of the storm with highest interaction with the ocean, regarding
 329 thermodynamic exchanges (Emanuel, 2003).

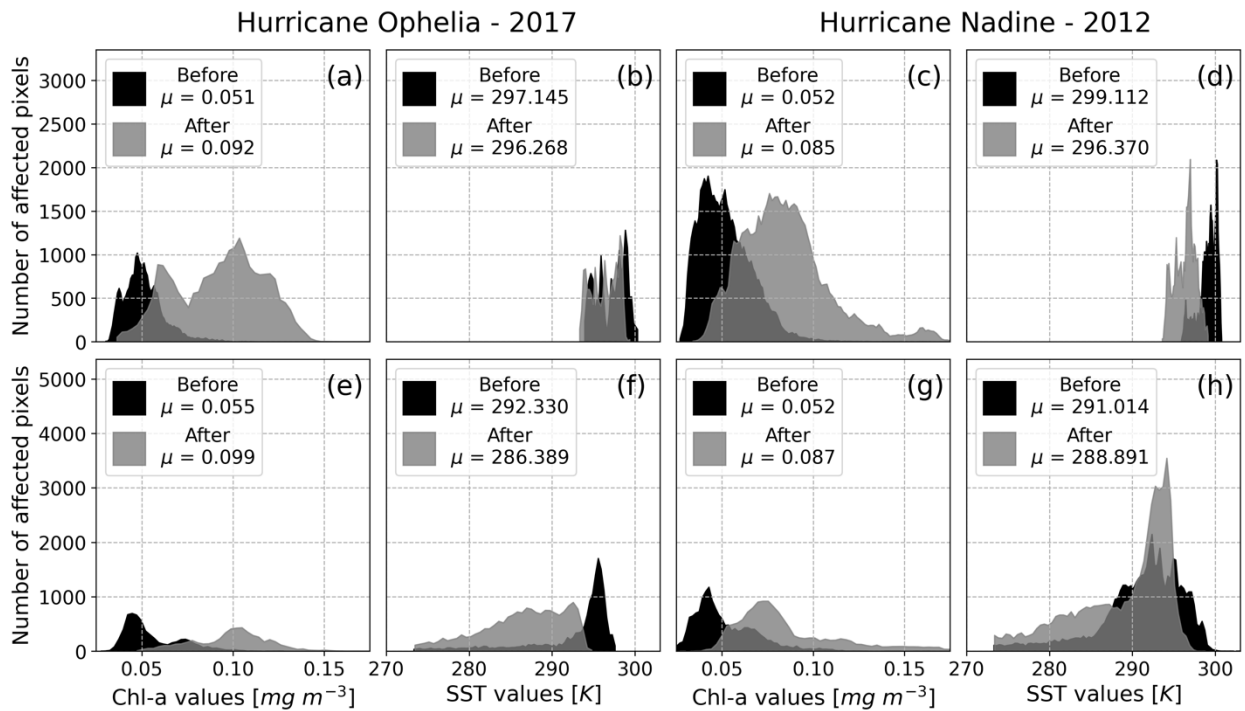
330 As a further insight to Ophelia's interaction with the ocean surface, Fig. S3 shows the mean modulus of wind stress
 331 on the surface, by day of analysis (Fig. S2a) and by Ophelia's 6-hour observations (Fig. S2b). Marked in both these
 332 plots are the analysed periods in corresponding colours and marker type to Fig. 6, these plots exceed the original study
 333 region, in order to fully encompass the TCs entire lifetime. There is a significant relation between the increased mean
 334 modulus of the wind stress and the evolution of the TC in time. This increase may be related to the increase in the
 335 storm's intensity, as Ophelia reaches its maximum intensity, so does the observed interaction with the ocean,
 336 decreasing afterwards as the storm moves north-eastward and undergoes post-tropical transition. This observed
 337 interaction with the ocean might be the reason for the maximum induced anomaly of Chl-a being observed at the end
 338 of Ophelia's passage over the study region, inducing the mixing of the superficial layer.



339
 340 **Figure 7 - Case study for Hurricane Nadine, in 2012, with the left panel the same as in Fig. 6. For Nadine, plots (b) and (c)**
 341 **pertain to the average induced Chl-a and SST anomalies, respectively, based on the amount of superposition verified in**
 342 **each pixel.**

343 Hurricane Nadine's (2012) case study shows very different behaviour and impact during its lifetime to that of
 344 Hurricane Ophelia. In this case, we present scatter plots of the averaged induced anomalies for the areas (Figs. 7b and

345 7c) corresponding to the superposition of pixels, i.e., the number of repeated observations inside the 34-kt isotach due
 346 to storms track geometry (as seen in Fig. 7a). The conclusions drawn regarding the Chl-a and SST induced anomalies
 347 are similar and significant in this case study: The more time the TC spent over a certain area the more this area became
 348 affected by its passage, with large anomalies registered in both variables (over 0.040 mg m^{-3} and -3.500 K for Chl-a and
 349 SST, respectively), and all cases being positive (negative), for Chl-a (SST). It is possible to hypothesise that the
 350 translation speed also had a relevant role in these results, with a slower TC (Nadine was one of the slowest TCs in this
 351 study, as seen by the closer observations in Fig. 7a and by Figs. 4 and 5) spending more time over a region and
 352 therefore producing larger anomalies.



353
 354 **Figure 8 – Comparison between interpolated “cloud-free” data (top row), and non-interpolated data (bottom row), for**
 355 **Hurricanes Ophelia (2017) and Nadine (2012). Values for non-interpolated data were obtained with the same methodology**
 356 **as the ones presented before and represent the exact same days of analysis. Mean values for each histogram are presented,**
 357 **with black histograms representing the situation before the TC and the grey ones the situation after.**

358 For these two case studies, we considered an additional quality assessment exercise, by comparing the interpolated
 359 “cloud-free” data to similar non-interpolated datasets. Figure 8 shows the histograms obtained for Ophelia and Nadine
 360 for the situations before and after the TC, independently, since non-interpolated data cannot be correctly subtracted as
 361 corresponding pixels may not be available. Overall, and despite the different number of observations considered, the
 362 Chl-a presents the same average response between the different types of data for both TCs, with non-interpolated data
 363 having an observed mean increase of 0.044 mg m^{-3} for Ophelia (Fig. 8e) compared to 0.041 mg m^{-3} for interpolated
 364 data (Fig. 8a), with these values representing the difference in the mean values shown in Fig. 8. Likewise, non-
 365 interpolated data reveals an increase of 0.035 mg m^{-3} for Nadine (Fig. 8g), compared to 0.033 mg m^{-3} for interpolated

366 data (Fig. 8c). Looking at the histograms, the shape of the data itself does not differ too much between the different
367 types, with peaks more or less located over the same values and distributions ranging the same values. However, for
368 the SST variable, despite both TC's present relatively similar decreases between both types of data, the non-
369 interpolated data has a wider range of values, and the peaks do not correspond so closely. This, however, may be due
370 to the process of data collation. In this process, some pixels are averaged with incorrect ones, resulting in unrealistic
371 values in some areas. This can be identified by the unrealistic SST seen in Figs. 8f and 8h, with values that do not
372 support TC development around 18-19°C and, so far as reaching 0°C. Nonetheless, interpolated SST data does show
373 the less uncertainty as verified before as the process of interpolating the data fixes this issue (Fig. S1).

374 **Final remarks**

375 The current study provides the first general assessment of the bio-physical oceanic response to the passage of TCs in
376 a relatively low cyclonic activity area such as the region near the Azores archipelago. It is important to stress the
377 efficiency of identifying the precise timing and associated spatial impacts of all TCs using remotely sensed products
378 that rely on interpolated areas to fill existing gaps due to cloud coverage or lack of satellite imagery.

379 Over the Azores region, it was generally identified the existence of a bio-physical response after the passage of a TC
380 was identified from the analysis of Chl-a and SST datasets, which produced signatures of positive Chl-a and negative
381 SST induced anomalies. This signature is more intense for the SST analysis, in which the passage of a TC results in
382 nearly all observed pixels to have a negative (i.e., cooling) induced anomaly. On average, TCs produced positive
383 anomalies in the order of 0.050 mg m⁻³ regarding Chl-a and a mean SST cooling of 1.615 K.

384 The more powerful TCs tend to produce more intense bio-physical oceanic responses, which agree with previous
385 literature on the topic (Chacko, 2019; Price, 1981; Price et al., 1994). TC translation speed was also found to be
386 associated with the induced anomalies, although the relationship was found to be positive and significant in the case
387 of Chl-a while it was not significant at the 95 % statistical confidence level for SST. The impacted area was also found
388 to be significantly linked to the oceanic response. However, the sensitivity to the impacted area can rise due to several
389 other factors: slower TCs impact larger areas (due to track geometry); more intense TCs impact larger areas (Knaff et
390 al., 2014); and TCs nearing post-tropical transition are generally larger (Knaff et al., 2014). These effects, either
391 individually or combined, can affect the induced anomalies at different levels. Additionally, the oceanic response was
392 found to be increased later in the season, with significant relation in both variables, this may be due to the seasonal
393 variability of the variables themselves, as the normal climatological values for that time of the year is exceeded in
394 exceptional TC conditions (Amorim et al., 2017; Lima et al., 2021) and the oceanic response may help the impacted
395 area return to expected values in both variables, in respect to that time of the year.

396 Two particular case studies were evaluated in further detail concerning hurricanes Ophelia (2017) and Nadine (2012).
397 Hurricane Ophelia was a particular case as it corresponds to the only major hurricane in this study region and had
398 almost its entire track inside this area. Ophelia showed strong induced anomalies for both Chl-a and SST variables.
399 Regarding Chl-a, Ophelia had a stronger impact towards the end of its track within the region, revealing that its
400 intensity played a key role in inducing Chl-a anomalies, with the mean modulus of wind stress revealing a positive

401 and significative relation to the evolution of the storm and therefore its intensity. On the other hand, Ophelia had a
402 stronger impact on the SST in its cyclogenesis, probably related to ocean-atmosphere thermodynamic exchanges
403 during its maturing. Hurricane Nadine, one of the slowest TCs in this study, showed more prominent anomalies,
404 especially regarding SST. In this case, considering the low translational speed of Nadine, the objective was to study
405 the impact that consecutive overlaid observations had on the induced anomalies. It is evident through this analysis that
406 the impact increases with the number of superposed observations, implying that Nadine's slow translation speed and
407 particular track geometry played a key role in creating such anomalies.

408 This study allowed for both the quality control of the remotely sensed "cloud-free" Chl-a and SST multi-sensor
409 products by comparing them to similar non-interpolated products, and in the sense that it identified expected changes
410 in the variables in areas covered by TC clouds and established crucial relations with some principal TC aspects. Future
411 studies should aim to understand the inherent physical mechanisms that affect the ocean during and after the passage
412 of a TC to better comprehend the associated induced anomalies.

413 **Code and Data availability**

414 All code and raw data used to support the conclusion of this article will be made available by the authors, without
415 undue reservation.

416 **Acknowledgements**

417 Research by Miguel M. Lima was supported by the Portuguese Science Foundation (FCT) through the project
418 "DiscoverAZORES", PTDC/CTA-AMB/28511/2017. The authors would like to thank the anonymous reviewers for
419 their thoughtful comments, suggestions, and efforts towards improving this work.

420 **Author Contribution**

421 Miguel M. Lima: Conceptualization, methodology, software, validation, formal analysis, investigation, writing –
422 original draft, review and editing. Célia M. Gouveia: Validation, supervision, writing – review and editing. Ricardo
423 M. Trigo: Validation, supervision, writing – review and editing, funding acquisition.

424 **Declaration of Interests**

425 The authors declare that they have no known competing financial interests or personal relationships that could have
426 appeared to influence the work reported in this paper.

427 **References**

428 Amorim, P., Perán, A. D., Pham, C. K., Juliano, M., Cardigos, F., Tempera, F., and Morato, T.: Overview of the
429 ocean climatology and its variability in the Azores region of the North Atlantic including environmental
430 characteristics at the seabed, *Frontiers in Marine Science*, 4, 56, doi:10.3389/fmars.2017.00056, 2017.

431 Baatsen, M., Haarsma, R. J., Van Delden, A. J., and de Vries, H.: Severe Autumn Storms in Future Western Europe
432 with a Warmer Atlantic Ocean, *Clim. Dyn*, 45 (3-4), 949–964, doi:10.1007/s00382-014-2329-8, 2015.

433 Caldeira, R., and Reis, J. C.: The Azores confluence zone. *Frontiers in Marine Science*, 4, 37,
434 doi:10.3389/fmars.2017.00037, 2017.

435 Chen, S., Elsberry, R. L., and Harr, P. A.: Modelling interaction of a tropical cyclone with its cold wake, *J. Atmos.*
436 *Sci.*, 74(12), 3981-4001, doi:10.1175/JAS-D-16-0246.1, 2017.

437 Chacko, N.: Differential chlorophyll blooms induced by tropical cyclones and their relation to cyclone
438 characteristics and ocean pre-conditions in the Indian Ocean. *J. Earth Syst. Sci.*, 128(7), 1-11. doi:10.1007/s12040-
439 019-1207-5, 2019.

440 CMEMS: ESA SST CCI and C3S reprocessed sea surface temperature analyses. Retrieved from
441 [https://resources.marine.copernicus.eu/?option=com_csw&view=details&product_id=SST_GLO_SST_L4](https://resources.marine.copernicus.eu/?option=com_csw&view=details&product_id=SST_GLO_SST_L4_REP_OBSERVATIONS_010_024)
442 [_REP_OBSERVATIONS_010_024](https://resources.marine.copernicus.eu/?option=com_csw&view=details&product_id=SST_GLO_SST_L4_REP_OBSERVATIONS_010_024), 2021a.

443 CMEMS: Global ocean chlorophyll, PP and PFT (copernicus-globcolour) from satellite observations: Monthly and
444 daily interpolated (reprocessed from 1997). Retrieved from
445 https://resources.marine.copernicus.eu/?option=com_csw&view=details&product_id=OCEANCOLOUR_GLO_CHL_L4_REP_OBSERVATIONS_009_082,
446 [_L_L4_REP_OBSERVATIONS_009_082](https://resources.marine.copernicus.eu/?option=com_csw&view=details&product_id=OCEANCOLOUR_GLO_CHL_L4_REP_OBSERVATIONS_009_082), 2021b.

447 Dickey, T., Frye, D., McNeil, J., Manov, D., Nelson, N., Sigurdson, D., ... and Johnson, R.: Upper-ocean
448 temperature response to Hurricane Felix as measured by the Bermuda Testbed Mooring, *Mon. Weather Rev.*,
449 126(5), 1195-1201, doi:10.1175/1520-0493(1998)126<1195:UOTRTH>2.0.CO;2, 1998.

450 Donlon, C. J., Martin, M., Stark, J., Roberts-Jones, J., Fiedler, E., and Wimmer, W.: The operational sea surface
451 temperature and sea ice analysis (OSTIA) system, *Proc. SPIE*, 116, 140-158, doi:10.1016/j.rse.2010.10.017, 2012.

452 Emanuel, K., Tropical Cyclones. *Annu. Rev. Earth Pl. Sc.*, 31 (1), 75–104,
453 doi:10.1146/annurev.earth.31.100901.141259, 2003.

454 Garnesson, P., Mangin, A., Fanton d'Andon, O., Demaria, J., and Bretagnon, M.: The CMEMS GlobColour
455 chlorophyll a product based on satellite observation: multi-sensor merging and flagging strategies, *Ocean Sci.*,
456 15(3), 819-830, doi:10.5194/os-15-819-2019, 2019.

457 Good, S., Fiedler, E., Mao, C., Martin, M. J., Maycock, A., Reid, R., ... and Worsfold, M.: The current configuration
458 of the OSTIA system for operational production of foundation sea surface temperature and ice concentration
459 analyses, *Remote Sens-Basel.*, 12(4), 720, doi:10.3390/rs12040720, 2020.

460 Haarsma, R. J., Hazeleger, W., Severijns, C., de Vries, H., Sterl, A., Bintanja, R., ..., and van den Brink, H. W.:
461 More Hurricanes to Hit Western Europe Due to Global Warming, *Geophys. Res. Lett.*, 40, 1783–1788,
462 doi:10.1002/grl.50360, 2013.

463 Hart, R. E., and Evans, J. L.: A climatology of the extratropical transition of Atlantic tropical cyclones, *J. Climate*,
464 14(4), 546-564, doi:10.1175/1520-0442(2001)014<0546:ACOTET>2.0.CO;2, 2001.

465 Holton, J. R., and Hakim, G. J., *An Introduction to Dynamic Meteorology*, 5th ed., Vol. 88. San Diego, CA:
466 Academic Press, Elsevier, doi:10.1119/1.1987371, 2012.

467 Kawai, Y., and Wada, A.: Detection of cyclone-induced rapid increases in chlorophyll-a with sea surface cooling in
468 the northwestern Pacific Ocean from a MODIS/SeaWiFS merged satellite chlorophyll product, *Int. J. Remote Sens.*,
469 32(24), 9455-9471, doi:10.1080/01431161.2011.562252, 2011.

470 Knaff, J. A., Longmore, S. P., and Molenar, D. A.: An objective satellite-based tropical cyclone size climatology, *J.*
471 *Climate*, 27(1), 455-476, doi:10.1175/JCLI-D-13-00096.1, 2014.

472 Knapp, K. R., Kruk, M. C., Levinson, D. H., Diamond, H. J., and Neumann, C. J.: The International Best Track
473 Archive for Climate Stewardship (IBTrACS), *B. Am. Meteorol. Soc.*, 91 (3), 363–376,
474 doi:10.1175/2009BAMS2755.1, 2010.

475 Kossin, J. P., Knapp, K. R., Olander, T. L., and Velden, C. S.: Global Increase in Major Tropical Cyclone
476 Exceedance Probability over the Past Four Decades, *P. Natl. A. Sci USA*, 117 (22), 11975–11980,
477 doi:10.1073/pnas.1920849117, 2020.

478 Krasnopolsky, V., Nadiga, S., Mehra, A., Bayler, E., and Behringer, D.: Neural networks technique for filling gaps
479 in satellite measurements: Application to ocean color observations, *Comput. Intel. Neurosc.*, 2016, 29,
480 doi:10.1155/2016/6156513, 2016.

481 Lavergne, T., Sørensen, A. M., Kern, S., Tonboe, R., Notz, D., Aaboe, S., ... and Pedersen, L. T.: Version 2 of the
482 EUMETSAT OSI SAF and ESA CCI sea-ice concentration climate data records, *The Cryosphere*, 13(1), 49-78,
483 doi:10.5194/tc-13-49-2019, 2019.

484 Lima, M. M. , Hurduc, A., Ramos, A. M. and Trigo, R. M.: The Increasing Frequency of Tropical Cyclones in the
485 Northeastern Atlantic Sector, *Front. Earth Sci.*, 9:745115, doi: 10.3389/feart.2021.745115, 2021.

486 Liu, X., Wang, M., and Shi, W.: A study of a Hurricane Katrina–induced phytoplankton bloom using satellite
487 observations and model simulations, *J. Geophys. Res-Oceans*, 114(C3), doi:10.1029/2008JC004934, 2009.

488 Maneesha, K., Murty, V. S. N., Ravichandran, M., Lee, T., Yu, W., and McPhaden, M. J.: Upper ocean variability in
489 the Bay of Bengal during the tropical cyclones Nargis and Laila, *Prog. Oceanogr.*, 106, 49-61,
490 doi:10.1016/j.pocean.2012.06.006, 2012.

491 Merchant, C. J., Le Borgne, P., Roquet, H., and Legendre, G.: Extended optimal estimation techniques for sea
492 surface temperature from the Spinning Enhanced Visible and Infra-Red Imager (SEVIRI), *Proc. SPIE*, 131, 287-297,
493 doi:10.1016/j.rse.2012.12.019, 2013.

494 Pan, J., Huang, L., Devlin, A. T., and Lin, H.: Quantification of typhoon-induced phytoplankton blooms using
495 satellite multi-sensor data. *Remote Sens-Basel*, 10(2), 318, doi:10.3390/rs10020318, 2018.

496 Pearce, R. P.: The physics of hurricanes. *Phys. Technol.*, 18(5), 215, 1987.

497 Price, J. F.: Upper ocean response to a hurricane. *J. Phys. Oceanogr.*, 11(2), 153-175, doi:10.1175/1520-
498 0485(1981)011<0153:UORTAH>2.0.CO;2, 1981.

499 Price, J. F., Sanford, T. B., and Forristall, G. Z.: Forced stage response to a moving hurricane. *J. Phys. Oceanogr.*,
500 24(2), 233-260, doi:10.1175/1520-0485(1994)024<0233:FSRTAM>2.0.CO;2, 1994.

501 Ramsay, H.: *The Global Climatology of Tropical Cyclones*. Oxford Research Encyclopedia of Natural Hazard
502 Science. Victoria, Australia: Oxford University Press, doi:10.1093/acrefore/9780199389407.013.79, 2017.

503 Saha, K., Zhao, X., Zhang, H., Casey, K. S., Zhang, D., Baker-Yeboah, S., ... and Relph, J. M.: AVHRR Pathfinder
504 version 5.3 level 3 collated (L3C) global 4km sea surface temperature for 1981-Present, NOAA National Centers for
505 Environmental Information, dataset, doi:10.7289/v52j68xx, 2018.

506 Sathyendranath, S., Brewin, R. J. W., Brockmann, C., Brotas, V., Calton, B., Chuprin, A., ... and Platt, T.: An
507 ocean-colour time series for use in climate studies: the experience of the Ocean-Colour Climate Change Initiative
508 (OC-CCI), *AH S. Sens.*, 19(19), 4285, doi:10.3390/s19194285, 2019.

509 Sathyendranath, S., Jackson, T., Brockmann, C., Brotas, V., Calton, B., Chuprin, A., ... and Platt, T.: ESA Ocean
510 Colour Climate Change Initiative (Ocean_Colour_cci): Version 5.0 Data, NERC EDS Centre for Environmental
511 Data Analysis, 19 May 2021, doi:10.5285/1d8e7a109c0244aaad713e078fd3059a, 2021.

512 Saulquin, B., Gohin, F., and Fanton d'Andon, O.: Interpolated fields of satellite-derived multi-algorithm
513 chlorophyll-a estimates at global and European scales in the frame of the European Copernicus-Marine Environment
514 Monitoring Service. *J. of Oper. Oceanogr.*, 12(1), 47-57, doi:10.1080/1755876X.2018.1552358, 2019.

515 Shropshire, T., Li, Y., and He, R.: Storm impact on sea surface temperature and chlorophyll a in the Gulf of Mexico
516 and Sargasso Sea based on daily cloud-free satellite data reconstructions, *Geophys. Res. Letters*, 43(23), 12-199,
517 doi:10.1002/2016GL071178, 2016.

518 Subrahmanyam, B., Rao, K. H., Srinivasa Rao, N., Murty, V. S. N., and Sharp, R. J.: Influence of a tropical cyclone
519 on chlorophyll-a concentration in the Arabian Sea, *Geophys. Res. Letters*, 29(22), 22-1,
520 doi:10.1029/2002GL015892, 2002.

521 Taylor, H. T., Ward, B., Willis, M., and Zaleski, W.: *The saffir-simpson hurricane wind scale*. Atmospheric
522 Administration: Washington, DC, USA., 2010.

523 Walker, N. D., Leben, R. R., and Balasubramanian, S.: Hurricane-forced upwelling and chlorophyll-a enhancement
524 within cold-core cyclones in the Gulf of Mexico, *Geophys. Res. Letters*, 32(18), doi:10.1029/2005GL023716, 2005.

- 525 Zhang, J., Lin, Y., Chavas, D. R., and Mei, W.: Tropical cyclone cold wake size and its applications to power
526 dissipation and ocean heat uptake estimates. *Geophys. Res. Letters*, 46(16), 10177-10185,
527 doi:10.1029/2019GL083783, 2019.
- 528 Zheng, Z. W., Ho, C. R., and Kuo, N. J.: Importance of pre-existing oceanic conditions to upper ocean response
529 induced by Super Typhoon Hai-Tang. *Geophys. Res. Letters*, 35(20), doi:10.1029/2008GL035524, 2008.